## COMMUNICATION

Check for updates

# Unbalanced MOF-on-MOF growth for the production of a lopsided core–shell of MIL-88B@MIL-88A with mismatched cell parameters†

Dooyoung Kim, Gihyun Lee, Sojin Oh and Moonhyun Oh [ID] *

**The unbalanced MOF-on-MOF growth of MIL-88A on the MIL-88B template, where both MOFs have a similar three-dimensional hexagonal structure but with mismatched cell parameters, results in the formation of an atypical lopsided core–shell of MIL-88B@MIL-88A with an off-centered core. The formation mechanism of the lopsided core–shell of MIL-88B@MIL-88A is verified *via* monitoring the growth process.**

Metal–organic frameworks (MOFs) or coordination polymers (CPs) are very useful materials for many practical applications, such as gas storage, separation, sensing, and catalysis, owing to their diversity in components and unique structural features.[1–6] Moreover, the construction of hybrid MOF materials, which contain more than two different materials and/or structures, is of great interest not only for fundamental curiosity but also for practical applications. Hybrid MOFs are considered to be more beneficial materials, because the weak point of MOFs can be overcome and the strength of the MOFs can be reinforced by preparing their hybrids.[7–10] Typically, hybrid MOFs can be constructed by either conjugating a MOF material with other functional materials such as magnetic particles, polystyrene, silica, and nanocatalysts,[10–15] or integrating more than two kinds of MOF components or MOF materials.[1,16–25]

The mixing of more than two different metal ions or organic linkers during the construction of MOFs can result in hybrid MOFs with an excellent property.[1,16–18] For example, Yaghi and co-workers reported the production of ultrahigh porous MOFs by using mixed organic linkers.[1] As another route to the integration of MOFs, a MOF-on-MOF growth strategy is an excellent approach to form well-defined hybrid MOFs, such as core–shell or layered MOFs, with a heterogeneous interface between the two MOFs.[7,8,19–25] For example, Kitagawa and

co-workers reported a sequential functionalized core–shell type MOF for selective adsorption.[19] Zhou and co-workers reported the preparation of a core–shell type hybrid MOF of PCN-222@Zr-BPDC with mismatched cell parameters.[21] In addition, we demonstrated the construction of core–shell or layered MOF particles through nanoscale isotropic or anisotropic MOF-on-MOF growth.[24] In general, the integration of two MOFs with matched cell parameters[7,8,19,20] is frequently performed and results in the isotropic growth of the second MOF. However, MOF-on-MOF growth with mismatched cell parameters[21–25] is more challenging and typically results in the anisotropic growth of the second MOF on the template MOF. In this work, we demonstrated the formation of an atypical lopsided core–shell of MIL-88B@MIL-88A *via* unbalanced MOF-on-MOF growth. Despite the large overall mismatch in the cell parameters of MIL-88A and MIL-88B due to the incorporation of different organic linkers, the similarity in the *ab* plane within the core and shell enables abnormal anisotropic MOF-on-MOF growth. The formation mechanism of the lopsided core–shell was verified by monitoring the samples at different time points by electron microscopy analyses.

First, nano-scale hexagonal rods of MIL-88B (Fig. 1a) were prepared from the solvothermal reaction of 1,4-benzenedicarboxylic acid ($H_2BDC$) and $Fe(NO_3)_3$ in accordance with a reported method.[26] MIL-88B has a three-dimensional (3D) hexagonal structure, where tri-metallic building units ($Fe_3O$) are connected by $BDC^{2-}$ to form a final 3D hexagonal structure with a chemical composition of $[Fe_3O(BDC)_3(H_2O)_2(NO_3)]_n$ (Scheme 1). Subsequently, the resulting hexagonal rods of MIL-88B were used as a template (or a seed) to enable the growth of MIL-88A for the formation of the core–shell type hybrid of MIL-88B@MIL-88A. Even though MIL-88A has a 3D hexagonal structure and topology similar to the MIL-88B template, the cell parameters of MIL-88A ($a = 11.18$ Å, $c = 14.68$ Å, $V = 1500$ Å$^3$)[27] are significantly different to those of MIL-88B ($a = 11.05$ Å, $c = 18.99$ Å, $V = 1980$ Å$^3$),[27] because a considerably short organic linker of fumaric acid is involved in the growth of MIL-88A, compared with $H_2BDC$ required for MIL-88B (Scheme 1). However, both MOFs have similar *a* cell parameters.

*Department of Chemistry, Yonsei University, 50 Yonsei-ro, Seodaemun-gu, Seoul 120-749, Korea. E-mail: moh@yonsei.ac.kr; Fax: +82 2 364 7050; Tel: +82 2 2123 5637*

Fig. 1   SEM images of (a) the MIL-88B template, (b) pure MIL-88A obtained in the absence of the MIL-88B template, and (c) lopsided core–shell of MIL-88B@MIL-88A obtained in the presence of the MIL-88B template. (d) STEM image of the lopsided core–shell of MIL-88B@MIL-88A. High-magnification (e–h) SEM and (i–l) STEM images showing several types of lopsided core–shell. Newly grown MIL-88A portions are highlighted in orange in (e–h). The numbers of core–shell, empty shell and naked core counted from several SEM images were 154, 123 and 106 out of 383.



Scheme 1   Schematic representation of the preparation of the lopsided core–shell of MIL-88B@MIL-88A. Ball-and-stick representation for MIL-88B. MIL-88A has a similar 3D hexagonal structure and topology to the MIL-88B template; however, the cell parameters of MIL-88A are significantly different to those of MIL-88B, because a considerably short organic linker (fumaric acid) is involved in the growth of MIL-88A, compared with $H_2BDC$ required for MIL-88B.

A successive solvothermal reaction of fumaric acid and $Fe(NO_3)_3$ in the presence of the MIL-88B template (hexagonal rods) was conducted. Scanning electron microscopy (SEM) images of the resulting product revealed the formation of hexagonal rods similar to the pure MIL-88B and MIL-88A (Fig. 1c). The products were larger than in the initial MIL-88B template (Fig. 1a), but smaller than in the pure MIL-88A rods (Fig. 1b) generated from a similar solvothermal reaction of fumaric acid and $Fe(NO_3)_3$ in the absence of the MIL-88B template. The size distributions of MIL-88B, MIL-88A and MIL-88B@MIL-88A measured from the SEM images are summarized in Fig. S3 (ESI†). In addition, high-magnification SEM images revealed the formation of atypical lopsided core–shell particles of MIL-88B@MIL-88A, which are generated from the unbalanced MOF-on-MOF growth of the secondary MOF

(MIL-88A) onto the surface of the initial MOF (MIL-88B) template (Fig. 1e–h). The scanning transmission electron microscopy (STEM) images of the products also revealed the formation of a lopsided core–shell of MIL-88B@MIL-88A, as shown in the shaded images (Fig. 1d and i–l). In the lopsided core–shell particles, the MIL-88B core was generally located off the center due to the unbalanced growth of the MIL-88A shell, as clearly shown in high-magnification SEM and STEM images (Fig. 1e–l). For example, core–shell particles, with the core located at the end of the particle (Fig. 1e, g, i and k), at the bottom of the particle (Fig. 1h and l), or between two newly grown MIL-88A portions (Fig. 1e and f), and sometimes empty MIL-88A shell particles after detaching the core portions (Fig. 1f and j) were observed. On the other hand, the formation of a well-defined core–shell of MIL-88A@MIL-88B was not observed from the reaction of $H_2BDC$ and $Fe(NO_3)_3$ in the presence of the MIL-88A template (Fig. S4, ESI†).

The growth of MIL-88A onto MIL-88B should be advantageous compared to generating pure MIL-88A particles after MIL-88A seed formation by itself. As evidence to support this speculation, the resulting amount of MIL-88A in the absence of the MIL-88B template was found to be considerably low (0.74 mg). However, the MIL-88B template induced fast and efficient generation of MIL-88A. Indeed, the resulting amount of MIL-88A (2.53 mg after subtracting the initial weight of the template) in the presence of the MIL-88B template was much larger than that produced in the absence of the MIL-88B template. The non-significant formation of pure MIL-88A particles during the MOF-on-MOF growth also supported this speculation (Table S1, ESI†). Despite the large

Fig. 2 SEM images monitoring the formation of the lopsided core–shell of MIL-88B@MIL-88A. The SEM images were acquired for the samples obtained from the reaction solution at different times (a) 0 min (initial template), (b) 2 min, (c) 4 min, (d) 6 min, (e) 8 min, and (f) 10 min. Newly grown MIL-88A portions are highlighted in orange in the magnified SEM images. (g) Mechanism for the unbalanced MOF-on-MOF growth of MIL-88A onto the MIL-88B template for the production of the lopsided core–shell of MIL-88B@MIL-88A.

mismatch in the cell parameter $c$ (26%) and cell volume (28%), a relatively well-matched $a$ (and thus $b$ because it is a hexagonal structure) cell parameter (1.2% mismatch) will allow efficient anisotropic MOF-on-MOF growth in the $c$ direction. Upon initiating the growth of a MIL-88A material onto some parts of the template, the continued growth of MIL-88A on those parts should be favorable compared to the uniform growth of the MIL-88A material onto the entire surface of the template; thus, eventually, this process results in the unbalanced growth and formation of lopsided MIL-88B@MIL-88A.

To understand the formation mechanism of the atypical lopsided MIL-88B@MIL-88A, the formation process was monitored by acquiring the SEM and STEM images of the samples obtained at different time points (Fig. 2 and Fig. S5, ESI†). Overall, the size of the products increased with increasing reaction time due to the continued growth of the MIL-88A shell.

Particularly, the SEM and STEM images of the samples acquired at the beginning of the reaction (2 min) showed the initiation of MOF-on-MOF growth by the formation of MIL-88A seeds on the template surface; typically, the initiation of the seed formation occurred at the end of the template (Fig. 2b, MIL-88A and MIL-88B have well-matched $a$ and $b$ cell parameters and it is therefore easy to initiate growth at the $ab$ plane at the end of the templates). Next, the SEM and STEM images of the samples acquired after 4 min indicated the unbalanced growth of MIL-88A mostly at the end of the templates, as shown in Fig. 2c. During this time, well-defined pointed hexagonal shapes of the newly grown materials were observed (magnified images in Fig. 2c). The SEM images of the samples acquired at the middle of the reaction (6 min) showed a noticeable growth of the second MOF (MIL-88A) onto the template. The SEM image acquired at the end of the reaction (8 and 10 min) clearly showed several types of lopsided MIL-88B@MIL-88A, where most of the MIL-88B template was wrapped by the newly grown MIL-88A (Fig. 1 and 2e, f). The relative ratios between MIL-88B and MIL-88A within the samples obtained at different time points are summarized in Table S2 (ESI†). In addition, further growth of the MIL-88A shell on the MIL-88B template was observed from the reaction in the presence of more precursors and the reaction resulted in an almost covered large core–shell (Fig. S6, ESI†).

The formation of the MIL-88A shell on the surface of MIL-88B was confirmed from the powder X-ray diffraction (PXRD) pattern and selected area electron diffraction (SAED) pattern of the resulting product. First, the PXRD pattern of lopsided MIL-88B@MIL-88A showed two obvious characteristic sets for the MIL-88B core and MIL-88A shell (Fig. 3). The peaks at $2\theta = 11.05°$ and $12.05°$ in the PXRD pattern of lopsided MIL-88B@MIL-88A were assigned to the (101) and (002) planes of the MIL-88A shell, whereas the peaks at $2\theta = 10.41°$ and $20.90°$ were assigned to the (101) and (202) planes of the MIL-88B core. All other peaks for the MIL-88B core and MIL-88A shell were well-matched to those of the pure MIL-88B template and MIL-88A rod. The PXRD peaks attributed to the MIL-88B core were relatively weak due to the predominant MIL-88A shell. Moreover, the unit cell parameters calculated from the PXRD patterns by whole pattern fitting (MDI Jade 9.0 software) were $a = 10.84$ Å and $c = 19.22$ Å for the MIL-88B template and $a = 11.03$ Å and $c = 14.71$ Å for pure MIL-88A. Both had well-matched $a$ (and hence $b$) cell parameters (1.7% mismatch). The unit cell parameters of the core ($a = 10.92$ Å and $c = 19.33$ Å) and shell ($a = 11.02$ Å and $c = 14.70$ Å, 0.9% $a$ cell parameter mismatch) portions within the lopsided MIL-88B@MIL-88A calculated from the PXRD pattern by whole pattern fitting were well-matched with those obtained from pure MIL-88B and MIL-88A. The SAED patterns of pure MIL-88B and MIL-88A indicated $d_{002}$ values of 0.96 and 0.75 nm, respectively, which represent the $c$ cell parameters of MIL-88B and MIL-88A of 19.2 and 15.0 Å, respectively (Fig. 4). Lastly, the SAED pattern acquired from a portion of the newly grown shell of lopsided MIL-88B@MIL-88A showed a $d_{002}$ value of 0.74 nm, indicating that this is MIL-88A (Fig. 4c).

In conclusion, we demonstrated the formation of an atypical lopsided core–shell of MIL-88B@MIL-88A, where the MIL-88B
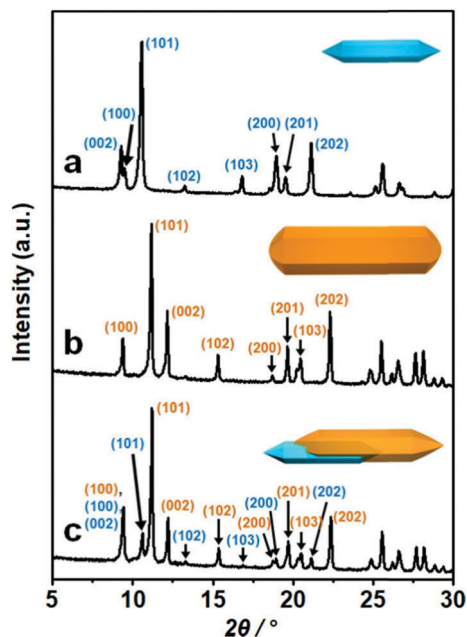
Fig. 3 PXRD patterns of (a) the MIL-88B template, (b) pure MIL-88A, and (c) the lopsided core–shell of MIL-88B@MIL-88A. Blue and orange represent MIL-88B and MIL-88A, respectively.



Fig. 4 TEM images (top) and SAED patterns (bottom) of (a) the MIL-88B template, (b) pure MIL-88A, and (c) the lopsided core–shell of MIL-88B@MIL-88A obtained from the region marked with circles.

core is located off the center, *via* unbalanced MOF-on-MOF growth. Despite the large overall mismatch in the cell parameters between the MIL-88B core and MIL-88A shell, the growth of MIL-88A onto the MIL-88B template occurred in an unbalanced (anisotropic) manner, owing to their similar *a* and *b* cell parameters. Detailed analysis of the growth process of MIL-88A onto the MIL-88B template clearly revealed the unique formation mechanism of lopsided MIL-88B@MIL-88A, initiating MOF-on-MOF growth by the formation of MIL-88A seeds at the end of the template, efficient unbalanced growth of MIL-88A in the *c*-direction, and wrapping of some part of the MIL-88B core. The MIL-88B template accelerated the generation of MIL-88A; however, atypical lopsided MIL-88B@MIL-88A

was generated due to the mismatched cell parameters, but with some similarity between the MIL-88B core and MIL-88A shell. This study may offer a viable route to the preparation of unique hybrid MOF materials.

## Conflicts of interest

There are no conflicts to declare.

## Notes and references

1 H. Furukawa, N. Ko, Y. B. Go, N. Aratani, S. B. Choi, E. Choi, A. Ö. Yazaydin, R. Q. Snurr, M. O'Keeffe, J. Kim and O. M. Yaghi, *Science*, 2010, **329**, 424–428.
2 O. K. Farha, A. Ö. Yazaydin, I. Eryazici, C. D. Malliakas, B. G. Hauser, M. G. Kanatzidis, S. T. Nguyen, R. Q. Snurr and J. T. Hupp, *Nat. Chem.*, 2010, **2**, 944–948.
3 Z. R. Herm, B. M. Wiers, J. A. Mason, J. M. van Baten, M. R. Hudson, P. Zajdel, C. M. Brown, N. Masciocchi, R. Krishna and J. R. Long, *Science*, 2013, **340**, 960–964.
4 W. Cho, H. J. Lee, G. Choi, S. Choi and M. Oh, *J. Am. Chem. Soc.*, 2014, **136**, 12201–12204.
5 L. He, Y. Liu, J. Liu, Y. Xiong, J. Zheng, Y. Liu and Z. Tang, *Angew. Chem., Int. Ed.*, 2013, **52**, 3741–3745.
6 O. Kozachuk, I. Luz, F. X. Llabrés i Xamena, H. Noei, M. Kauer, H. B. Albada, E. D. Bloch, B. Marler, Y. Wang, M. Muhler and R. A. Fischer, *Angew. Chem., Int. Ed.*, 2014, 53, 7058–7062.
7 T. Li, J. E. Sullivan and N. L. Rosi, *J. Am. Chem. Soc.*, 2013, **135**, 9984–9987.
8 H. Ji, S. Lee, J. Park, T. Kim, S. Choi and M. Oh, *Inorg. Chem.*, 2018, **57**, 9048–9054.
9 Y. Lee, S. Kim, J. K. Kang and S. M. Cohen, *Chem. Commun.*, 2015, **51**, 5735–5738.
10 Z. Li and H. C. Zeng, *J. Am. Chem. Soc.*, 2014, **136**, 5631–5639.
11 T. Wehner, K. Mandel, M. Schneider, G. Sextl and K. Müller-Buschbaum, *ACS Appl. Mater. Interfaces*, 2016, **8**, 5445–5452.
12 H. J. Lee, W. Cho and M. Oh, *Chem. Commun.*, 2012, **48**, 221–223.
13 C. Jo, H. J. Lee and M. Oh, *Adv. Mater.*, 2011, **23**, 1716–1719.
14 B. Rungtaweevoranit, J. Baek, J. R. Araujo, B. S. Archanjo, K. M. Choi, O. M. Yaghi and G. A. Somorjai, *Nano Lett.*, 2016, **16**, 7645–7649.
15 J. Park and M. Oh, *Nanoscale*, 2017, **9**, 12850–12854.
16 H. Furukawa, U. Müller and O. M. Yaghi, *Angew. Chem., Int. Ed.*, 2015, **54**, 3417–3430.
17 H. J. Lee, J. We, J. O. Kim, D. Kim, W. Cha, E. Lee, J. Sohn and M. Oh, *Angew. Chem., Int. Ed.*, 2015, **54**, 10564–10568.
18 Y. Jiao, J. Pei, D. Chen, C. Yan, Y. Hu, Q. Zhang and G. Chen, *J. Mater. Chem. A*, 2017, **5**, 1094–1102.
19 K. Hirai, S. Furukawa, M. Kondo, H. Uehara, O. Sakata and S. Kitagawa, *Angew. Chem., Int. Ed.*, 2011, **50**, 8057–8061.
20 T. Ishiwata, A. Michibata, K. Kokado, S. Ferlay, M. W. Hosseini and K. Sada, *Chem. Commun.*, 2018, **54**, 1437–1440.
21 X. Yang, S. Yuan, L. Zou, H. Drake, Y. Zhang, J. Qin, A. Alsalme and H.-C. Zhou, *Angew. Chem., Int. Ed.*, 2018, **57**, 3927–3932.
22 S. Furukawa, K. Hirai, K. Nakagawa, Y. Takashima, R. Matsuda, T. Tsuruoka, M. Kondo, R. Haruki, D. Tanaka, H. Sakamoto, S. Shimomura, O. Sakata and S. Kitagawa, *Angew. Chem., Int. Ed.*, 2009, **48**, 1766–1770.
23 V. Chernikova, O. Shekhah, I. Spanopoulos, P. N. Trikalitis and M. Eddaoudi, *Chem. Commun.*, 2017, **53**, 6191–6194.
24 H. J. Lee, Y. J. Cho, W. Cho and M. Oh, *ACS Nano*, 2013, **7**, 491–499.
25 S. Choi, T. Kim, H. Ji, H. J. Lee and M. Oh, *J. Am. Chem. Soc.*, 2016, **138**, 14434–14440.
26 W. Cho, S. Park and M. Oh, *Chem. Commun.*, 2011, **47**, 4138–4140.
27 S. Surblé, C. Serre, C. Mellot-Draznieks, F. Millange and G. Férey, *Chem. Commun.*, 2006, 284–286.